Published in final edited form as:
Nano Lett. 2011 February 9; 11(2): 814–819. doi:10.1021/nl104141g.

Chimeric ferritin nanocages for multiple function loading and multimodal imaging

Xin Lin[†,⊥], **Jin Xie**[†,⊥], **Gang Niu**[†], **Fan Zhang**[†], **Haokao Gao**[†], **Min Yang**[†], **Qimeng Quan**[†], **Maria A. Aronova**[‡], **Guofeng Zhang**[‡], **Seulki Lee**[†], **Richard Leapman**[‡], and **Xiaoyuan Chen**[*,†]

[†] Laboratory of Molecular Imaging and Nanomedicine (LOMIN), National Institute of Biomedical Imaging and Bioengineering (NIBIB), National Institutes of Health (NIH), Bethesda, Maryland 20892

[‡] Laboratory of Cellular Imaging and Macromolecular Biophysics, NIBIB, NIH, Bethesda, Maryland 20892

Abstract

Nanomaterials provide large surface areas, relative to their volumes, on which to load functions. One challenge, however, has been to achieve precise control in loading multiple functionalities. Traditional bioconjugation techniques, which randomly target the surface functional groups of nanomaterials, have been found increasingly inadequate for such control--a drawback which may substantially slow down or prohibit the translational efforts. In the current study, we evaluated ferritin nanocages as candidate nanoplatforms for multifunctional loading. Ferritin nanocages can be either genetically or chemically modified to impart functionalities to their surfaces, and metal cations can be encapsulated in their interiors by association with metal binding sites. Moreover, different types of ferritin nanocages can be disassembled under acidic condition and reassembled at pH of 7.4, providing a facile way to achieve function hybridization. We were able to use combinations of these unique properties to produce a number of multifunctional ferritin nanostructures with precise control of their composition. We then studied these nanoparticles, both *in vitro* and *in vivo*, to evaluate their potential suitability as multimodality imaging probes. A good tumor targeting profile was observed, which was attributable to both the enhanced permeability and retention (EPR) effect and biovector mediated targeting. This, in combination with the generalizability of the function loading techniques, promises ferritin particles as a powerful nanoplatfom in the era of nanomedicine.

Keywords

ferritin nanocage; multimodality molecular imaging; positron emission tomography; near-infrared fluorescence imaging; integrin; RGD peptide

The idea of multimodality imaging has recently gained popularity[1, 2]. The rationale arises from the notion of improving the quality and accuracy of disease management by combining

[*]To whom correspondence should be addressed, Shawn.Chen@nih.gov.
[⊥]Both authors contributed equally to this work.

Supporting Information
Additional information regarding the expression and purification of Fn and R-Fn, preparation of C-Fn, synthesis of chimeric ferritin nanocages, cell binding assay, small animal PET and NIRF optical imaging studies, immunofluorescence staining, results of DLS analysis of R-Fn, and results of ex vivo imaging of excised tumors. This material is available free of charge via the Internet at http://pubs.acs.org.

the complementary strengths of multiple imaging techniques. For instance, many efforts have been dedicated to the development positron emission tomography/computed tomography (PET/CT) imaging[3–5], a fused technique that permits simultaneous acquisition of functional and high-resolution anatomical information. Similarly, near-infrared fluorescence (NIRF) imaging and PET can be an interesting combination, which provides both *in vivo* imaging interrogation and *ex vivo* validation so as to minimize the chances of misdiagnosis[6, 7]. Such a transition to multimodal imaging poses a challenge to the design and synthesis of new generations of imaging probes. It requires that a targeting motif be integrated in a compact and controllable way with multiple imaging tags--something that is difficult to achieve with traditional biomaterials such as peptides and proteins. The emergence of nanotechnology, however, is expected to provide solutions to such challenges. With large ratios of surface-area-to-volume and multiple binding sites, nanomaterials can be loaded with a number of motifs[8–10]. However, the monotonicity of the binding sites to a great extent limits the reproducibility and quality control of the function loading. Despite the maturity of bioconjugation techniques, it remains a challenge to achieve multifunctional nanoprobes with accurate control, while not affecting their stability, targeting specificity or bioactivity.

Ferritin is a family of proteins found in different forms in most living organisms. Each ferritin is made of 24 subunits, which self-assemble to form a cage-like nanostructure, with external and internal diameters of 12 and 8 nm, respectively[11]. This unique architecture provides two interfaces--one outside and one inside--for possible functional loading[12]. The outer surface of ferritin can be chemically or genetically modified with functional motifs, and the cavity of the ferritin can bind a wide range of metals with high affinity[12–16]. For instance, there were efforts of introducing biovector onto ferritin surface and following that, evaluating the targeting of the conjugates toward C32 melanoma cancer cells[12]. Also, it was reported that ferritin nanocage could load gadolinium (Gd) into its cavity and then function as a MRI contrast agent to depict tumor endothelial cells[17]. Recently, it was found that the assembly of ferritin, despite its rigidness under physiological condition, is pH dependent[18, 19]. The nanoarchitecture can be broken down in an acidic environment and restored, almost intactly, by retuning the pH to 7.4. These unique properties, especially the diversity of loading mechanisms, make ferritin a potentially powerful nanoplatform on which to construct multifunctional nanoagents for imaging; the necessary related studies, however, have not been reported.

We present here our efforts to load RGD4C, Cy5.5 and ^{64}Cu simultaneously onto heavy chain ferritins to produce nanoprobes with both PET and NIRF functionalities for tumor imaging. RGD4C peptide (CDCRGDCFC) has been studied as a biovector for targeting integrin $\alpha_v\beta_3$, whose up-regulation has been found to be implicated in tumor angiogenesis of a variety of cancer types[20, 21]. ^{64}Cu and Cy5.5 are imaging motifs with PET and NIRF functionalities, respectively. The combination of RGD4C peptide, ^{64}Cu and Cy5.5 will enable the loaded nanoplatforms to: 1) target tumor, mediated by RGD-integrin interaction and the enhanced permeability and retention (EPR) effect, 2) report the tumor location (via ^{64}Cu and Cy5.5), and 3) reveal the distribution of the probes, at the cellular level, in the tumor area (via Cy5.5). Such multiple loading can be done by using traditional bioconjugation techniques, where the dye molecules, chelators (such as DOTA) and RGD are anchored to the ferritin surface by conjugation with the surface amines. However, issues of cross-motif interference will inevitably arise, and dissimilarities among the motifs will make controlling the composition of the final products extremely difficult. Instead of taking such a route, we capitalized on the versatile loading mechanisms of ferritin nanoparticles to arrive at a hybrid nanostructure (Figure 1). In brief, we first prepared two sets of heavy chain ferritins (Fn), one Cy5.5 labeled (C-Fn) and the other RGD4C labeled (R-Fn), as the building blocks. Notably, Cy5.5 was chemically coupled to the ferritin surface, but RGD4C

was genetically introduced by following a previously published protocol[12]. For Cy5.5 conjugation, we were able to achieve a 1:1 Cy5.5 to ferritin ratio by adjusting the reaction conditions. We then incubated these two types of ferritins, C-Fn and R-Fn, in an acidic environment (pH = 2) to break down the nanostructure to discrete subunits (confirmed by dynamic light scattering, Figure S1). We then adjusted the pH back to 7.4, to reconstitute the ferritin nanoparticles into hybrid structures (Figure S2).

To optimize the hybrid structure, we started with C-Fn/R-Fn mixtures at different R/C ratios (R/C = 2:1, 1:1 and 1:2) and prepared hybrid ferritins (hereafter referred to as RC-Fn). We then analyzed the products with size exclusion chromatography (SEC) and compared the results to R-Fn and C-Fn alone. As shown in Figure 2, R-Fn and C-Fn alone had a retention time of 46.7 min and 48.4 min, respectively. All the reconstituted formulas displayed retention peaks that lay between these two, with a tendency for higher C-Fn composition to yield longer retention times (retention times of 46.88, 46.93 and 47.75 m for formulas with R/C ratios of 2:1, 1:1 and 1:2, respectively), thereby confirming the successful formation of the hybrid ferritins.

To study how the hybridization affected the ability of nanocages to bind integrin, we performed a series of cell-binding assays with MDA-MD-435 cells, using ^{125}I-echistatin as the competitive binding ligand (Figure 3a). C-Fn alone showed no binding towards integrin. R-Fn, on the other hand, showed an IC_{50} of 2.9 nM (based on ferritin monomer concentration, the same with the other formulas), which is about one order of magnitude lower than RGD4C alone (24.44 nM)[22]. Such a dramatic increase in binding affinity is attributed to the multivalent effect, which we and others have observed previously with other RGD multimers[23–25]. Due to the dilution of C-Fn, all the RC-Fn showed decreased binding affinity compared with R-Fn, with IC_{50} values of 13 nM, 5.5 nM and 10 nM for R/C ratios of 2:1, 1:1 and 1:2, respectively. To our surprise, the highest binding affinity came from the formula with the R/C ratio of 1:1, rather than from the one with the highest R/C ratio (2:1). The detailed mechanism is unknown at this stage and will be a subject of further investigation. Nonetheless, the optimized formula (R/C = 1:1) was selected for further evaluation.

We then added the third functionality, ^{64}Cu, to our nanoplatform. ^{64}Cu is a radioisotope, actively used in PET imaging. Traditionally, the loading of ^{64}Cu has been achieved by pre-conjugating chelators, such as DOTA and NOTA, onto biovectors, after which $^{64}Cu^{2+}$ can be complexed with the chelators. In the current study, however, we exploited the possibility of direct loading of $^{64}Cu^{2+}$ into the ferritin nanostructures by harnessing the metal binding capability of ferritin. It was observed previously that the cavity of ferritin particles were capable of binding with divalent metal cations[11, 16]. Exploring the potential of this attribute in the context of radioisotope labeling and imaging, however, has not been reported.

The $^{64}Cu^{2+}$ was added to the mixture of C-Fn and R-Fn (R/C =1:1) in an acidic environment (pH = 2) (Figure 1). As with the previous preparation, we then adjusted the pH back to 7.4 to reform nanocages. The free $^{64}Cu^{2+}$ was removed by passing the reaction mixture through a PD-10 column (see the Methods section). A dose calibrator (Capintec) showed that 60% of the isotopes could be loaded into the ferritins in a typical loading. To investigate the durability of the loaded $^{64}Cu^{2+}$, we then subjected the $^{64}Cu^{2+}$ loaded RC-Fn to dialysis in both phosphate-buffered saline (PBS) and serum (fetal bovine serum, Invitrogen) and monitored the activity loss over time (see the Methods section in the Supplementary Information). We found that under both conditions, the radioisotopes were well retained in the nanocages (Figure 3b&c), with less than 10% of the isotopes (decay-corrected) released from the nanocages within an observation period of 24 h.

After confirming the formation of such tri-functional nanoarchitectures, we conducted *in vivo* validation experiment. In brief, the hybrid probes were injected intravenously into a U87MG glioma xenograft tumor model, and the tumor-bearing mice were imaged by both PET and NIRF. For PET studies, each mouse was injected with about 100 μCi of ^{64}Cu-RC-Fn via tail vein and the tomographic images were acquired on a Siemens Inveon microPET scanner at various time points post injection (p.i.) (see the Methods section in the Supplementary Information). The decay-corrected whole body images are shown in Figure 4. It can be seen that the intensities gradually accumulated in the tumor area within the first 24 h and then dropped slightly. By drawing 3-dimensional regions of interest (ROIs) over the images, we were able to quantify the probe uptakes in the tumor (Figure 5b), which were 6.4 ± 1.7, 7.5 ± 0.7, 8.1 ± 0.1 and 7.5 ± 0.1 %ID/g at 1, 4, 24 and 40 h p.i. (n = 3). Such a high tumor accumulation rate could be caused by two factors: RGD-integrin interaction and the EPR effect. To elucidate this, we injected a second group of mice with c(RGDyk) (0.5 mg per mouse) 30 min prior to the ^{64}Cu-RC-Fn injection. This pre-injection of c(RGDyk) did not lead to immediate blocking of tumor accumulation, as manifested by almost the same tumor uptake rate at the 1 h time point (6.4 ± 2.3 %ID/g). However, a continuous drop of activity was observed afterwards, with tumor uptakes of 5.9 ± 1.8, 6.0 ± 1.3 and 4.4 ± 0.7% ID/g, at 4, 24 and 40 h time points. This observation corroborates our hypothesis that both RGD-integrin targeting and the EPR effect were involved in the modulation of tumor retention. Hence, while the receptor mediated uptake was greatly inhibited in the presence of a blocking dose of RGD peptide, the EPR effect remained functioning to mediate the accumulation of activities in the tumor area. However, without specific interaction, probes were more susceptible to washout and lymphatic drainage, which could explain the continuous drop of activity. A similar tumor accumulating profile was also observed with NIRF imaging (Figure 4b). While a marginal difference was found between the nonblocking and the blocking groups at 1 h p.i., such a difference in tumor uptake continued to grow and it maximized at 40 h (1373.92 ± 320.08 vs. 442.30 ± 208.93 $10^6 \cdot \text{phot} \cdot \text{cm}^{-2} \cdot \text{s}^{-1}$ for the non-blocking and blocking groups at 40 h).

After the 40 h imaging, we sacrificed the mice and collected the tumors along with major organs for *ex vivo* PET (Figure 5a) and optical imaging (Figure S3). In accordance with the *in vivo* observation, we found a dramatic difference in tumor uptake between the blocking and non-blocking groups. Besides the high tumor accumulation of the probe, we found a great deal of intensities from the liver. To further investigate the distribution of the probes in the tumor area, we performed immunostaining of the tumor tissues (Figure 6). We found from the CD31 staining that in both groups there was accumulation of probes around the tumor vasculature, a pattern that could indicate EPR mediated tumor uptake. We then conducted β_3 staining to light up tumor vascular integrin $\alpha_v\beta_3$. We observed in the non-blocking group a very good correlation between the Cy5.5 signals (red, from the ferritin probes) and the FITC signals (green, from the integrin). Notably, the superimposition occurred on both tumor cells and on vasculature, in accordance with our previous observations with U87MG models[26, 27]. On the contrary, we found no correlation between β_3 staining and Cy5.5 activities in the blocking group. This once again validated our hypothesis that both RGD-integrin interaction and EPR effect had played a role in the accumulation of probes in tumor, while in the blocking group RGD-integrin interaction was efficiently inhibited by the pre-injection of c(RGDyK).

One critical topic in the design of a multifunctional nanogadget is how to control the loading of the motifs while minimizing their interference. Traditional nanoplatforms achieve function loading primarily with bioconjugation techniques. These methods have been incompetent in dealing with multiple-loading tasks, since most nanomaterials can afford only one kind of functional group on their surface. Taking the current study as an example, it may be possible to use traditional methods to achieve such multiple loading by, for

instance, simultaneously conjugating RGD, Cy5.5 and DOTA onto the lysine from the ferritin surface. However, it will then be very hard, if not impossible, to control the composition of the final products, since all three motifs are coupled via the same mechanism. In the current study, however, we loaded the motifs via three different mechanisms. The ^{64}Cu was directly loaded by capitalizing on the inherent metal binding capacity of ferritin. Instead of loading Cy5.5 and RGC4C simultaneously, we loaded them onto different sets of ferritins, and then integrated them into a hybrid nanostructure by harnessing the reconstitution capability of ferritins. Since we controlled, chemically and genetically, that each ferritin subunit would have one Cy5.5 or RGD4C, we were able to tune the composition of the final ferritins and, by so doing, manipulate their role as imaging probes. Specifically, we identified that one chimeric ferritin nanocage formula (R/C = 1:1) had an integrin $\alpha_v\beta_3$ affinity that is ~9 fold higher than RGD4C alone.

Although it was reported previously that metal cations can be loaded into the cavities of ferritin cages, using such a route to load radioisotopes has not been reported. It is acknowledged that there are three-fold hydrophilic channels in the ferritin nanocages, which connect the inside and outside of ferritins and serve as the paths (and the only paths) to allow the entrance of ions (such as Fe^{2+} and Cd^{2+}) into the cavity [28–30]. Analysis of the crystal structures of metal loaded ferritins has revealed that ions, such as Cd^{2+}, could be loaded into such channels, indicating the presence of a strong binding site for divalent cations in the center of the pores[30]. Considering the similar size of Cu^{2+} to Fe^{2+} and Cd^{2+}, we believe that the $^{64}Cu^{2+}$ was trapped and loaded into ferritin nanocages via the same route. And, due to the existence of a potential gradient along the channel[11], once loaded, the cations would find it hard to escape from the nanocages, and this perhaps explains the excellent stability of $^{64}Cu^{2+}$ in PBS and serum. Such a loading mechanism is highly favorable because: 1) there is no need to introduce chelators onto the surface of ferritin, 2) it is quick and efficient. As a matter of fact, we found that ^{64}Cu can be loaded directly into ferritins at pH = 6 without breaking down the nanostructures (data not shown), and 3) the loading is stable against environmental change. Since the isotopes are embedded in the center of the cavity, many potential influential factors, such as serum proteins in the circulation, do not have access to the radioisotopes. This, in combination with an intrinsic potential that points to the center of the nanocages, guarantees the stability of ^{64}Cu in the circulation.

The technique developed in this work can be readily extended to load other types of functionalities. Different targeting motifs can be easily introduced onto the surface of such a nanosystem to replace or assist RGD as a targeting motif. For example, it will be interesting to achieve ferritin-based RGD-bombesine hybrids of different ratios and evaluate their potentials in prostate cancer imaging[31, 32]. Additionally, radioisotopes other than $^{64}Cu^{2+}$ should be able to be loaded into ferritin nanoparticles via the same means. These include other radioisotopes with imaging functionalities, such as ^{68}Ga and ^{89}Zr, as well as isotopes with therapeutic functions, such as ^{177}Lu and ^{90}Y. In addition, since there are 24 subunits in each ferritin nanoparticle, it may be possible to construct more complicated nanostructures, such as quadruplicately or even quintuplicately loaded nanoplatforms. The related studies are currently underway.

In summary, we have demonstrated in the current study the loading of ferritin nanocages with RGD4C, Cy5.5 and ^{64}Cu ferritin achieves nanoplatforms with both integrin-targeting specificity and PET/NIRF imaging functionalities. The motifs were loaded via three different mechanisms and were integrated, by taking advantage of the reconstitution ability of ferritin, into a hybrid form of ferritin nanoparticles. Unlike the traditional conjugation methods, such a loading strategy minimizes interference among different docked motifs and enables accurate control over the composition of the final conjugates. The success of this

study has implications for on-going efforts to construct multimodal imaging probes and nanoparticulate theranostics.

Supplementary Material

Refer to Web version on PubMed Central for supplementary material.

Acknowledgments

This work was supported in part by the Intramural Research Program (IRP) of the National Institute of Biomedical Imaging and Bioengineering (NIBIB), NIH and the International Cooperative Program of National Science Foundation of China (NSFC) (81028009). J.X. is partially supported by an NIH Pathway to Independence Grant (K99/R00). S.L. acknowledges a National Research Council Research Associateship Award funded by the National Institute of Standards and Technology (NIST) and the IRP of NIBIB, NIH. We thank Dr. Henry S. Eden for proof-reading the manuscript.

References

1. Louie A. Chem Rev 110(5):3146–95. [PubMed: 20225900]
2. Cherry SR. Annu Rev Biomed Eng 2006;8:35–62. [PubMed: 16834551]
3. Hustinx R, Lucignani G. Eur J Nucl Med Mol Imaging 37(3):645–51. [PubMed: 20187296]
4. Zangheri B, Messa C, Picchio M, Gianolli L, Landoni C, Fazio F. Eur J Nucl Med Mol Imaging 2004;31(Suppl 1):S135–42. [PubMed: 15133636]
5. Schoder H, Larson SM, Yeung HW. J Nucl Med 2004;45(Suppl 1):72S–81S. [PubMed: 14736838]
6. Xie J, Chen K, Huang J, Lee S, Wang J, Gao J, Li X, Chen X. Biomaterials 31(11):3016–22. [PubMed: 20092887]
7. Lee S, Chen X. Mol Imaging 2009;8(2):87–100. [PubMed: 19397854]
8. Xie J, Lee S, Chen X. Adv Drug Deliv Rev.
9. Xie J, Huang J, Li X, Sun S, Chen X. Curr Med Chem 2009;16(10):1278–94. [PubMed: 19355885]
10. Lee S, Xie J, Chen X. Chem Rev 110(5):3087–111. [PubMed: 20225899]
11. Maham A, Tang Z, Wu H, Wang J, Lin Y. Small 2009;5(15):1706–21. [PubMed: 19572330]
12. Uchida M, Flenniken ML, Allen M, Willits DA, Crowley BE, Brumfield S, Willis AF, Jackiw L, Jutila M, Young MJ, Douglas T. J Am Chem Soc 2006;128(51):16626–33. [PubMed: 17177411]
13. Douglas T, Stark VT. Inorg Chem 2000;39(8):1828–30. [PubMed: 12526579]
14. Zhang L, Laug L, Munchgesang W, Pippel E, Gosele U, Brandsch M, Knez M. Nano Lett 10(1): 219–23. [PubMed: 20017497]
15. Hosein HA, Strongin DR, Allen M, Douglas T. Langmuir 2004;20(23):10283–7. [PubMed: 15518526]
16. Ueno T, Abe M, Hirata K, Abe S, Suzuki M, Shimizu N, Yamamoto M, Takata M, Watanabe Y. Journal of the American Chemical Society 2009;131(14):5094–100. [PubMed: 19317403]
17. Geninatti Crich S, Bussolati B, Tei L, Grange C, Esposito G, Lanzardo S, Camussi G, Aime S. Cancer Res 2006;66(18):9196–201. [PubMed: 16982763]
18. Santambrogio P, Levi S, Arosio P, Palagi L, Vecchio G, Lawson DM, Yewdall SJ, Artymiuk PJ, Harrison PM, Jappelli R, et al. J Biol Chem 1992;267(20):14077–83. [PubMed: 1629207]
19. Kang S, Oltrogge LM, Broomell CC, Liepold LO, Prevelige PE, Young M, Douglas T. J Am Chem Soc 2008;130(49):16527–9. [PubMed: 19554690]
20. Cai W, Niu G, Chen X. Curr Pharm Des 2008;14(28):2943–73. [PubMed: 18991712]
21. Cai W, Chen X. J Nucl Med 2008;49(Suppl 2):113S–28S. [PubMed: 18523069]
22. Hu Z, Luo F, Pan Y, Hou C, Ren L, Chen J, Wang J, Zhang Y. J Biomed Mater Res A 2008;85(3): 797–807. [PubMed: 17896765]
23. Li ZB, Cai W, Cao Q, Chen K, Wu Z, He L, Chen X. J Nucl Med 2007;48(7):1162–71. [PubMed: 17574975]

24. Xie J, Chen K, Lee HY, Xu C, Hsu AR, Peng S, Chen X, Sun S. J Am Chem Soc 2008;130(24): 7542–3. [PubMed: 18500805]
25. Montet X, Funovics M, Montet-Abou K, Weissleder R, Josephson L. J Med Chem 2006;49(20): 6087–93. [PubMed: 17004722]
26. Chen K, Xie J, Xu H, Behera D, Michalski MH, Biswal S, Wang A, Chen X. Biomaterials 2009;30(36):6912–9. [PubMed: 19773081]
27. Cai W, Chen K, Li ZB, Gambhir SS, Chen X. J Nucl Med 2007;48(11):1862–70. [PubMed: 17942800]
28. Levi S, Luzzago A, Franceschinelli F, Santambrogio P, Cesareni G, Arosio P. Biochem J 1989;264(2):381–8. [PubMed: 2690826]
29. Takahashi T, Kuyucak S. Biophys J 2003;84(4):2256–63. [PubMed: 12668434]
30. Hempstead PD, Yewdall SJ, Fernie AR, Lawson DM, Artymiuk PJ, Rice DW, Ford GC, Harrison PM. J Mol Biol 1997;268(2):424–48. [PubMed: 9159481]
31. Liu Z, Li ZB, Cao Q, Liu S, Wang F, Chen X. J Nucl Med 2009;50(7):1168–77. [PubMed: 19525469]
32. Li ZB, Wu Z, Chen K, Ryu EK, Chen X. J Nucl Med 2008;49(3):453–61. [PubMed: 18287274]

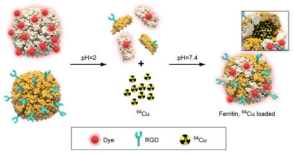

FIGURE 1.

Schematic illustration of the process of triple-loading. First, we introduced RGD4C and Cy5.5 onto the surfaces of two sets of ferritins, via genetic and chemical means. These two ferritins were then mixed and broken down into subunits at pH=2, and incubated with $^{64}CuCl_2$ to achieve radiolabeling. The pH was then adjusted back to 7.4 to facilitate the reformation of nanostructures. The reconstituted chimeric ferritin nanocages have both RGD4C and Cy5.5 on their surfaces and ^{64}Cu loaded in their cavities.

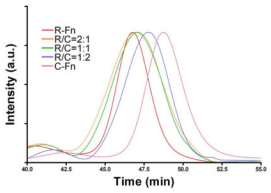

FIGURE 2.

Size exclusion chromatography analysis of the hybrid ferritins. R-Fn and C-Fn alone showed retention times of 46.7 min and 48.4 min, respectively. Increased proportion of Cy5.5 in the chimeric ferritins led to longer retention times.

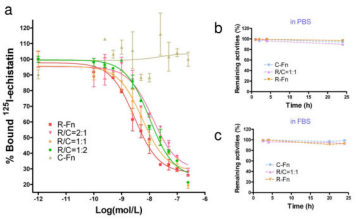

FIGURE 3.

a) Binding affinity assays on MDA-MB-435 cells with different ferritin formulas. b–c) Stability test with ^{64}Cu loaded ferritins in PBS or FBS. Less than 10% of the radioactivity was found to be released out of ferritin cages after 24 h incubation.

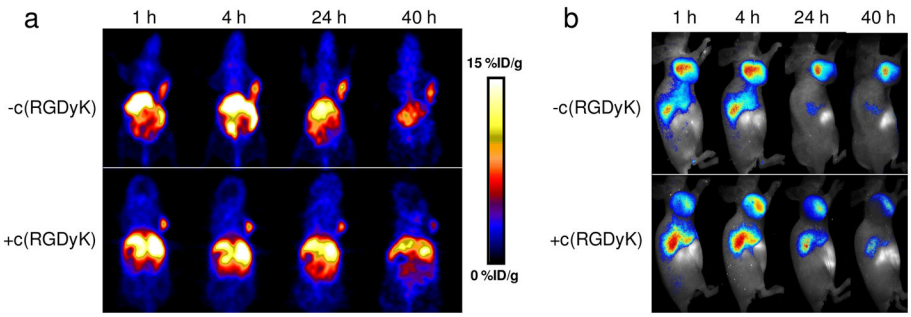

FIGURE 4.

In vivo a) PET and b) NIRF images after the administration of ferritin probes. In the comparison group, a blocking dose of c(RGDyK) was injected 30 min prior to the ferritin probe administration.

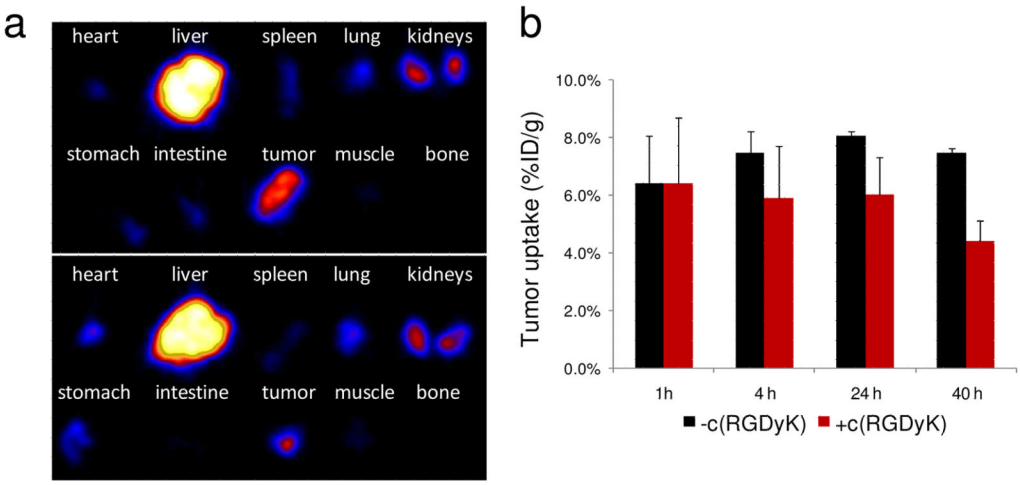

FIGURE 5.

a) *Ex vivo* PET imaging on tumors as well as major organs collected after the 40 h imaging. b) Tumor uptake assessed for ROIs from the *in vivo* PET imaging results.

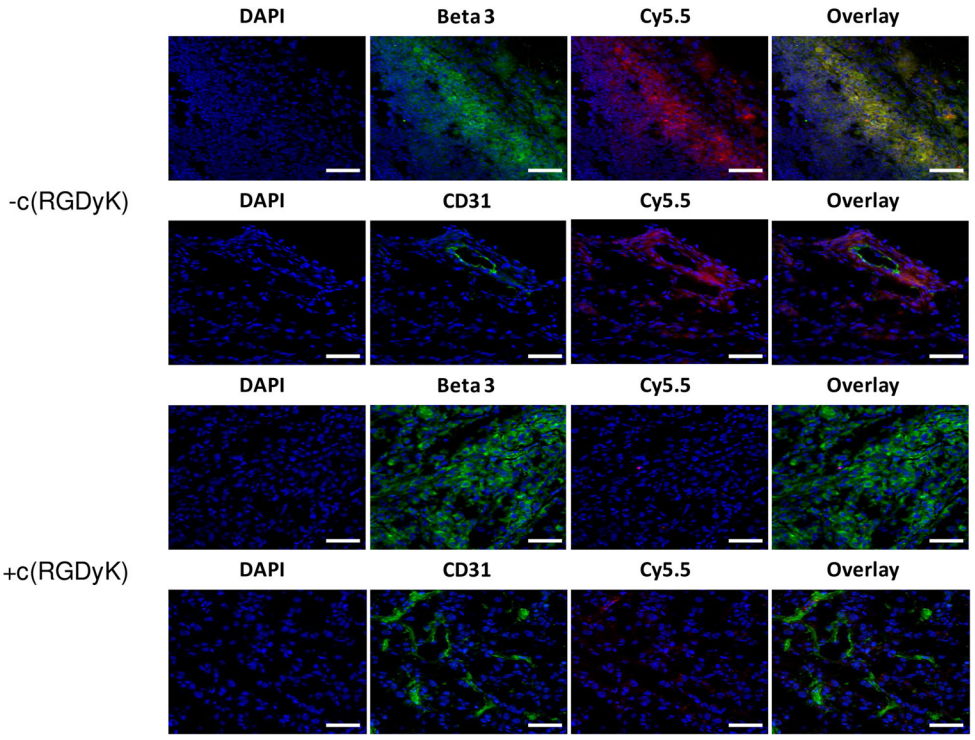

FIGURE 6.

Immunostaining results. Tumor tissues from both the blocking and non-blocking groups were subjected to CD31 staining and β_3 staining to elucidate the tumor accumulation mechanisms. Blue: DAPI; red: Cy5.5; green: FITC, for either vasculature (CD31) or integrin $\alpha_v\beta_3$ (β_3). Scale bar: 50 μm.